

Heat transport in the geostrophic regime of rotating Rayleigh-Bénard convection

Robert E. Ecke¹ and Joseph J. Niemela²

¹Center for Nonlinear Studies, Los Alamos National Laboratory, Los Alamos, NM 87545, USA

²International Center for Theoretical Physics, Strada Costiera 11, 34014 Trieste, Italy*

(Dated: July 10, 2018)

We report experimental measurements of heat transport in rotating Rayleigh-Bénard convection in a cylindrical convection cell with aspect ratio $\Gamma = 1/2$. The fluid was helium gas with Prandtl number $\text{Pr} = 0.7$. The range of control parameters was Rayleigh number $4 \times 10^9 < \text{Ra} < 4 \times 10^{11}$ and Ekman number $2 \times 10^{-7} < \text{Ek} < 3 \times 10^{-5}$ (corresponding to Taylor number $4 \times 10^9 < \text{Ta} < 1 \times 10^{14}$ and convective Rossby number $0.07 < \text{Ro} < 5$). We determine the crossover from weakly rotating turbulent convection to rotation dominated geostrophic convection through experimental measurements of the normalized heat transport Nu . The heat transport for the rotating state in the geostrophic regime, normalized by the zero-rotation heat transport, is consistent with scaling of $(\text{RaEk}^{-7/4})^\beta$ with $\beta \approx 1$. A phase diagram is presented that encapsulates measurements on the potential geostrophic turbulence regime of rotating thermal convection.

PACS numbers: 47.20.Bp, 47.32.-y, 47.54.+r

Thermal convection in the presence of rotation occurs in many geophysical contexts, including the Earth's mantle [1], oceans [2], planetary atmospheres such as Jupiter [3], and solar interiors [4]. It also remains a fundamental problem in fluid dynamics, balancing rotation and buoyancy in a simple system that can be studied theoretically [5], experimentally [6–11] and numerically [12, 13] with high precision. Thus, the problem of rotating thermal convection is of interest across a wide spectrum of scientific disciplines.

The parameters of rotating convection are $\text{Ra} = g\alpha\Delta T d^3 / \nu\kappa$ which measures the buoyant forcing of the flow, $\text{Ek} = \nu / (2d^2\Omega)$ which represents an inverse dimensionless rotation rate, and $\text{Pr} = \nu/\kappa$, where g is acceleration of gravity, ΔT is the temperature difference between top and bottom plates separated by distance d , ν and κ are the fluid kinematic viscosity and thermal diffusivity, respectively, and $\Omega = 2\pi f$ is the angular rotation about an axis parallel to gravity for rotation frequency f . Rotation can also be represented by the Taylor number $\text{Ta} = 1/\text{Ek}^2$ or by the convective Rossby number $\text{Ro} = \text{Ek} \sqrt{\text{Ra}/\text{Pr}}$ which reflects the ratio of rotational time to buoyancy time. Here we use the representation of Ek or Ro such that high dimensionless rotation rates correspond to small values of the rotational control parameter in the spirit of the asymptotic equation approach of expanding in a small variable [14]. The measured response of the system in this space of buoyant and rotational forcing is the Nusselt number, $\text{Nu} = \dot{Q}/(\lambda\Delta T)$ where \dot{Q} is the applied heater power through the fluid and λ is the thermal conductance of the fluid.

Much of the experimental work on rotating convection at high dimensionless rotation rates has focused on either the transition to convection where rotation-induced wall modes play an important role [7, 15] or the turbulent state far from onset where thermal boundary layers control heat transport [6, 8–11]. Recently, the numerical simulation [16, 17] of the appropriate equations of motion [14] in the asymptotic limit of high rotation rate has focused on the heat transport scaling above the convective onset but below the transition to boundary-layer controlled turbulence - a region that we will

refer to as geostrophic turbulence. Several predictions have been made for the scaling of heat transport in this regime with power laws in Rayleigh number, Ra , corresponding to $\text{Ra}^{3/2}$, based on numerical simulations [17], or Ra^3 based on dimensional arguments [18, 19]. The data in this regime are scarce and the range of Prandtl number, Pr , Ekman number Ek (proportional to the inverse of the angular rotation rate Ω), and Ra is very limited. In particular, the crossovers from buoyancy dominated turbulent convection (where rotation has no measurable effect) to rotation-influenced turbulent convection (dominated by thermal boundary layer development) to geostrophic turbulence (Ek small) have not been well investigated.

The experimental apparatus used for these studies has been described in detail previously [21, 22] so we include only essential details. The convection cell had a cylindrical geometry with height $d = 100$ cm and diameter 50 cm resulting in an aspect ratio $\Gamma = 1/2$. The working fluid was helium gas near its critical point at around 5.2K, and the range of Ra and Ek was controlled by a combination of variations of ΔT in the range 0.04 - 0.30 K at a mean cell temperature between 4.61 and 4.75 K and densities ρ of 0.00033, 0.00066, 0.0013, and 0.0018 g/cc. The Prandtl number was constant at $\text{Pr} = 0.7$. For most of the runs, f was fixed at the maximum for the apparatus corresponding to 0.167 Hz resulting in runs at constant Ek (and Ta). In one run, Ra was fixed and f varied between 0.0056 and 0.167 Hz. For all of the data, Nu was measured without rotation as a reference and is denoted Nu_0 . The data are reported in standard ratios of $\text{Nu}(\text{Ra}, \Omega)/\text{Nu}_0(\text{Ra}, 0)$, that to first order compensate for small systematic uncertainties, and also facilitates comparison to other data sets by providing a self-reference for the system that takes into account the possibility of small differences in static and/or dynamic boundary conditions, etc.

We measure the convective heat transport through the Nusselt number Nu and explore the crossover to geostrophic rotating turbulence over a parameter range $2 \times 10^{-7} < \text{Ek} < 3 \times 10^{-5}$ and $4 \times 10^9 < \text{Ra} < 4 \times 10^{11}$, corresponding to

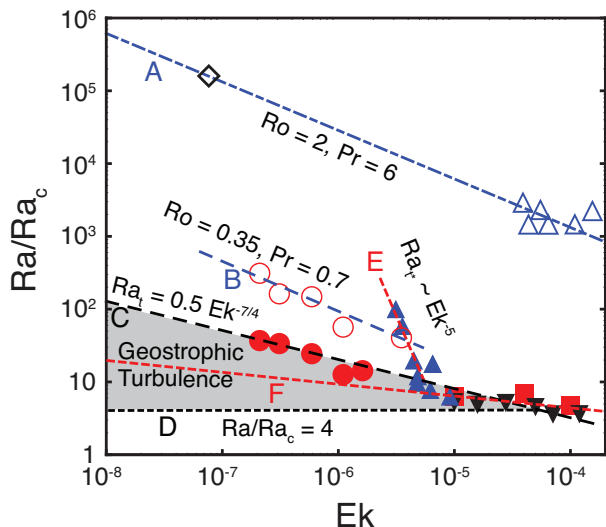


FIG. 1: Phase diagram of rotating convection in parameters Ra/Ra_c and Ek . Rotation first affects turbulent convection below line A for $Pr = 6$ ($Ro = 2$) and below line B for $Pr = 0.7$ ($Ro = 0.35$). The crossover to geostrophic turbulence is roughly independent of Pr (or depends on it very weakly) and occurs along line C where $Ra_t = 0.5Ek^{-7/4}$ and above line D which indicates $Ra/Ra_c = 4$ corresponding roughly to a regime of weakly non-linear convection near onset. Line E indicates a rapid change in the crossover for $Pr = 4.4$ corresponding to $Ra_{t*} \sim Ek^{-5}$. Line F is the upper limit of applicability of proposed Ra^3Ek^4 scaling corresponding to the relationship $Ra/Ra_c \lesssim Ek^{-1/6}$. Data are from [9] (solid square - red), [10, 20] (open and solid up triangles - blue), [11] (solid down triangles - black), [21] (open diamond - black), and this work (open and solid circles - red). The shaded region corresponds to states expected to show geostrophic turbulence.

a range of convective Rossby Number, $0.07 < Ro < 5$. We find that the crossover to buoyancy dominated turbulence has a strong Pr dependence whereas the crossover to geostrophic turbulence has, at most, a weak Pr dependence and, over a range of moderate Pr and more than 3 orders of magnitude in Ek , occurs for values of Ra consistent with $Ra_t = 0.5Ek^{-7/4}$. A summary of the resultant phase diagram based on a combination of our measurements with earlier measurements at larger Pr and Ek [9–11] (mostly water at different mean temperatures) is shown in fig. 1 where we normalize Ra by the rotation-dependent $Ra_c = 8.4Ek^{-4/3}$, representing linear stability values: in general, one needs $Ra/Ra_c \gg 1$ to achieve a strongly nonlinear turbulent state. The strong Pr dependence of the crossover from buoyancy-dominated to rotation-influenced thermal boundary layer turbulence is easily demonstrated by comparing lines A and B. Line C shows the extrapolation of our $Ra_t \sim Ek^{-7/4}$ curve to include the higher Pr data. The high Pr data are consistent with the $Ek^{-7/4}$ relationship for $8 \times 10^{-6} < Ek < \times 10^{-4}$. On the other hand, the high Pr data for smaller Ek [20] show an abrupt increase along line E with $Ra_{t*} \sim Ek^{-5}$, an apparently unnoticed feature of the high Pr data. We also show line F, the upper limit of self-consistency for arguments [19, 23] leading to $Nu \sim Ra^3Ek^4$,

which corresponds to $Ra/Ra_c \lesssim Ek^{-1/6}$ which we derive below. Finally, we find that the scaling of Nu with Ra in the geostrophic regime is consistent with a power law of order 1; no evidence for power-law scaling of $Nu \sim Ra^3$ [19] is found.

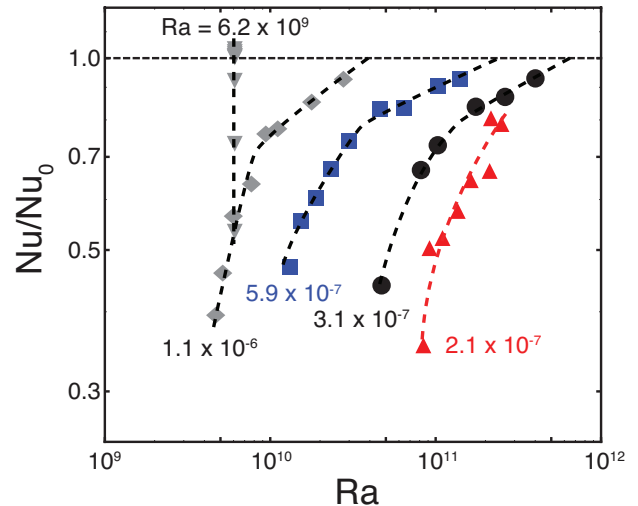


FIG. 2: (Color Online) Nu/Nu_0 vs Ra for constant Ek : 1.1×10^{-6} (solid diamond - gray), 5.9×10^{-7} (solid square - blue), 3.1×10^{-7} (solid circle - black), 2.1×10^{-7} (solid up triangle - red), and for constant $Ra = 6.2 \times 10^9$ (solid down triangle - gray). Dashed lines are guides to the eye.

As in earlier experiments [21] in this apparatus at much higher Ra and $Pr = 6$, $Nu/Nu_0 \leq 1$ for all parameters measured as shown in fig. 2. The data are for four different runs corresponding to constant Ek between 10^{-6} and 10^{-7} and one run at constant $Ra = 6.2 \times 10^9$. From these data, we determine the Ek dependent values of Ra where Nu/Nu_0 drops below 1. These transition values Ra_T are plotted in fig. 1 (line B) with an Ek dependence consistent with a constant $Ro \approx 0.35$. The data also suggest a second change in slope of the curves for smaller Ra but this behavior shows up more clearly if we scale the data so that they collapse onto a single curve.

One possibility for collapsing the data is to plot them in terms of Ro (proportional to $Ra^{1/2}Ek$ or equivalently $RaEk^2$) which we show in fig. 3. The collapse is reasonable although the DNS data [10] at much lower Ra are not captured well by this scaling. The collapse does suggest two ranges of behavior consisting of an initial decrease in Nu/Nu_0 with decreasing Ro starting at $Ro \approx 0.35$ and a second more rapid decrease starting at $Ro \approx 0.1$. Nu/Nu_0 has dropped to about 0.8 at this second decrease. The solid lines indicate power law curves corresponding to $Ro^{1/4}$ for the first decrease and $Ro^{3/2}$ for the faster decrease. No particularly strong conclusions can be drawn from these scalings but they are convenient for characterizing the form of the data. The lack of collapse of the DNS data at much lower Ra , however, anticipates that the scaling can be improved.

Recently, measurements in water with $Pr \approx 6$ were conducted [9] in which the crossover between the boundary-layer dominated turbulent state and convection with $Nu/Nu_0 < 1$

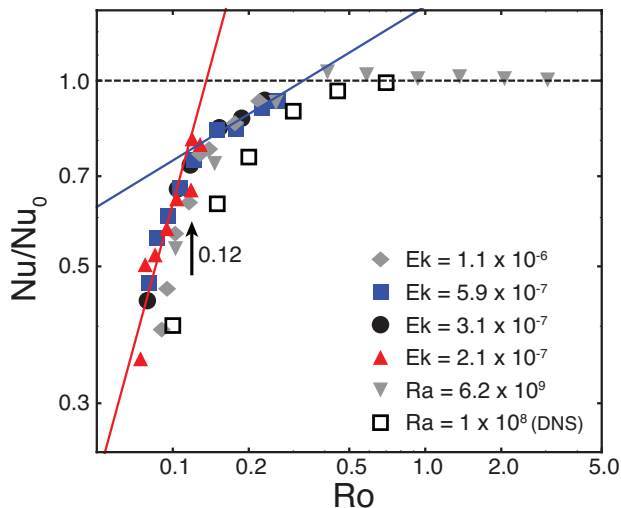


FIG. 3: (Color Online) Log-Log plot of Nu/Nu_0 vs Ro for constant Ek : 1.1×10^{-6} (solid diamond - gray), 5.9×10^{-7} (solid square - blue), 3.1×10^{-7} (solid circle - black), 2.1×10^{-7} (solid up triangle - red), and for constant Ra : 6.2×10^9 (solid down triangle - gray), DNS [10] - 1×10^8 (open square - black). The solid lines show approximate power law variations of the region $0.8 < Nu/Nu_0 < 1$ with $Ro^{1/4}$ (top, blue) and for $Nu/Nu_0 < 0.8$ with $Ro^{3/2}$ (bottom, red), respectively. Vertical arrow indicates approximate transition value $Ro = 0.12$.

was attributed to competing thermal and Ekman boundary layers. The resulting crossover was found to have the form $Ra_t = 1.4Ek^{-7/4}$, suggesting the scaling variable $Ra Ek^{7/4}$. We show the data normalized in this manner in fig. 4. The collapse for our data is better for this scaling with the DNS data now collapsed as well. The difference in the two scalings is rather small, i.e., $Ra Ek^2$ in fig. 3 compared to $Ra Ek^{7/4}$ in fig. 4. It takes the large difference in Ra for the DNS to differentiate the two scalings. A more recent analysis of the experimental water data [19] suggested that a better fit was to $Ra Ek^{3/2}$ but that does not fit our data very well. Furthermore, the DNS results also are then significantly shifted to the left of the experimental points. Indeed, to within our experimental uncertainties, we find $Ra_t = 0.5Ek^{-7/4}$ as plotted in the phase diagram in fig. 1. Interestingly this relationship fits the crossover estimates for data with higher Pr in the range 3-6 [9–11] and for $Ek > 4 \times 10^{-6}$ but with a lower prefactor than the 1.4 suggested earlier [9].

The power law straight lines in fig. 4 are consistent with those in fig. 3, yielding relationships of $Ra^{1/7}$ and $Ra^{2/3}$ for the slopes. Again these lines are drawn for the purposes of describing the data collapse and are over quite limited ranges of parameters. There is, however, no evidence for Ra^3 scaling.

Expanding on the limits for a geostrophic turbulence regime, numerical simulations [17] suggest that one needs Ra/Ra_c to be larger than about 4 to 6 to enter a regime of geostrophic turbulence. We denote this limit in fig. 1 as line D. One implication of this cutoff that can be drawn from the

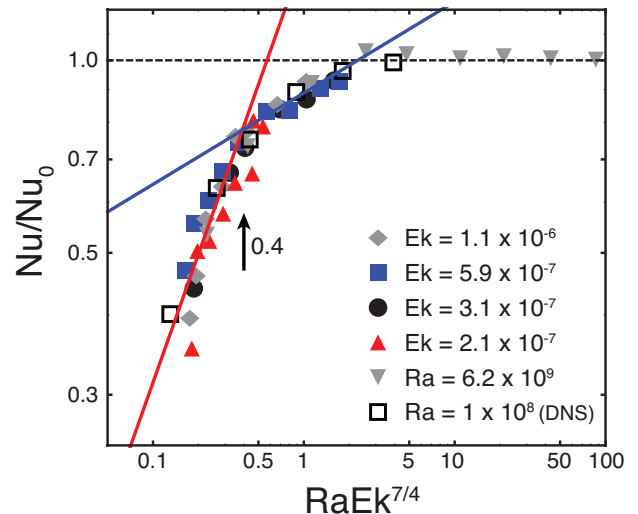


FIG. 4: (Color Online) Log-Log plot of Nu/Nu_0 vs $RaEk^{7/4}$ for constant Ek : 1.1×10^{-6} (solid diamond - gray), 5.9×10^{-7} (solid square - blue), 3.1×10^{-7} (solid circle - black), 2.1×10^{-7} (solid up triangle - red), and for constant Ra : 6.2×10^9 (solid down triangle - gray), DNS [10] - 1×10^8 (open square - black). The solid lines show approximate power law variations of the region $0.8 < Nu/Nu_0 < 1$ with $(RaEk^{7/4})^{1/7}$ (top, blue) and for $Nu/Nu_0 < 0.8$ with $(RaEk^{7/4})^{2/3}$ (bottom, red), respectively. Vertical arrow indicates approximate transition value $RaEk^{7/4} = 0.4$, slightly less than the best value of 0.5 that fits all the data.

phase diagram is that experiments at higher $Ek > 10^{-5}$ do not have a measurable range of geostrophic turbulence. At the lower end for the present experiments, the range of Ra/Ra_c available is ultimately limited by \dot{Q} and ΔT resolution. In principle, one would like measurements of Nu over a range of Ra such that $Ra_c \ll Ra \ll Ra_t$. This limit suggests that one needs $Ek < 10^{-7}$ to achieve a sufficient range to measure a decade of scaling of Nu with Ra in the geostrophic turbulence range and $Ek < 10^{-9}$ to approach two decades. This will be a stiff challenge for future experiments. In the present case, it is unclear whether our scaling of $Nu/Nu_0 \sim Ra^\beta$ with $\beta \approx 1$ is obtained far enough below Ra_t not to be influenced by that crossover; i.e., larger values of β are not completely ruled out by these measurements. Nevertheless, the data presented here have the lowest Ek (highest dimensionless rotation rate) and largest range that resolves the geostrophic turbulence range of experiments performed until now.

Another surprise in our phase diagram is the very steep Ek dependence of the apparent crossover to boundary layer rotation-influenced turbulent convection. These data were obtained in experiments [20] that were not designed to determine the low Ro crossover but instead concentrated on the crossover at higher Ra/Ra_c to rotation-free buoyancy driven turbulence. Measurements on that system indicated that the aspect ratio Γ plays a role in determining the upper boundary [24] and that there is a Pr dependence of the crossover [20] of approximately $Ro_c \sim Pr^{0.4}$. On the first point, the data at very high Ra in helium gas with $\Gamma = 0.5$ [21] suggest that the transition

remains at $Ro_c \approx 2$ independent of Γ so there may be Ra dependence since an implication of the measured Γ dependence [24] would be $Ro_c \approx 4$. Second, if we take lines A and B as describing the data for $Pr = 6$ and $Pr = 0.7$, respectively, the implied Pr dependence would be $Ro_c \sim Pr^{0.8}$ rather than the previously indicated $Pr^{0.4}$ dependence. Finally, coming back to the apparently rapid change in the turbulent crossover for $Ek < 8 \times 10^{-6}$, this feature is unexpected and entirely unexplained.

The last feature of note in our phase diagram in fig. 1 is the range of possible existence for a scaling range with $Nu \sim Ra^3 Ek^4$. The assumption of the marginal stability arguments leading to that scaling is that the stability of thin thermal boundary layers of width δ is the same as for the bulk rotating convection problem, namely that one can write [19]

$$Ra_c^\delta = \frac{Ra}{2} \left(\frac{\delta}{d} \right)^3 = BEk_\delta^{-4/3} = BEk^{-4/3} \left(\frac{\delta}{d} \right)^{8/3} \quad (1)$$

where $B = 8.4$ and the sub/superscript δ denotes the evaluation using δ rather than d . From this relationship, one solves for δ to yield $\delta/d = 2^{3/8} B^{3/8} Ra^{-3/8} Ek^{-4/8}$, which implies $Nu = d/(2\delta) \sim Ra^{3/8} Ek^{4/8}$. For this to hold, however, one needs $Ra_c^\delta > C$ where $C \gtrsim 1000$, i.e., that the boundary layer feels the effect of rotation rather than being effectively a non-rotating stability problem. In other words, $Ra_c^\delta \sim Ek_\delta^{-4/3}$ is only valid for $Ek \ll 1$ which is violated as δ decreases because $Ek_\delta \sim \delta^{-2}$. The resulting expression of the absolute upper limit of self consistency of this argument results from solving for Ra/Ra_c above to obtain

$$Ra/Ra_c \lesssim Ek^{-1/6}. \quad (2)$$

This condition is line F in fig. 1. Based on this estimate, it seems unlikely that one could observe this regime for $Ek > 10^{-5}$, with a solid decade of scaling only possible for $Ek < 10^{-9}$ and $Ek < 10^{-15}$ for two decades!

The phase diagram in fig. 1 suggests the following: 1) The transition from buoyancy dominated turbulent convection to rotation influenced turbulent convection depends sensitively on Pr and approximately scales as Ro . 2) The transition from rotation-influenced to rotation-dominated convection is best described by a transition relationship $Ra_t = 0.5Ek^{-7/4}$ with little or no Pr dependence. 3) The available range of Ra/Ra_c is insufficient to observe geostrophic turbulence scaling [17] or $Ra^3 Ek^4$ scaling [19] for $Ek > 10^{-5}$ which includes almost all of the data taken for water with $Pr \approx 5$ [6–11]. 4) Although our results for $Pr = 0.7$ lie on approximately the same transition line to geostrophic turbulence (line C) as the results at higher $Pr > 5$, there may be another branch of transitions (line E in fig. 1). 5) To observe a full decade of geostrophic turbulence scaling will require $Ek < 10^{-7}$ whereas a similar range for a possible $Ra^3 Ek^4$ range would need $Ek < 10^{-9}$.

There are thus many experimental and numerical challenges that need to be addressed to further characterize and extend the fascinating problem of rotating thermal convection.

We acknowledge important conversations with Keith Julien, Antonio Rubio and Geoffrey Vasil concerning predictions of numerical simulations. Contributions by Ecke were funded by the National Nuclear Security Administration of the U.S. Department of Energy at Los Alamos National Laboratory under Contract No. DE-AC52-06NA25396. We acknowledge the Elettra Synchrotron Laboratory, Trieste, for providing technical and logistical assistance and, in particular, we wish to thank Mr. Piergiorgio Tosolini.

* Corresponding Author: ecke@lanl.gov

- [1] G. Glatzmaier, R. Coe, L. Hongre, and P. Roberts, *Nature* **401**, 885 (1999).
- [2] J. Marshall and F. Schott, *Rev. Geophys.* **37**, 1 (1999).
- [3] M. Heimpel, J. Aurnou, and J. Wicht, *Nature* **438**, 193 (2005).
- [4] E. A. Spiegel, *Annu. Rev. Astron. Astrophys.* **9**, 323 (1971).
- [5] S. Chandrasekhar, *Hydrodynamic and Hydromagnetic Stability* (Oxford University Press, Oxford, 1961).
- [6] H. T. Rossby, *J. Fluid Mech.* **36**, 309 (1969).
- [7] F. Zhong, R. E. Ecke, and V. Steinberg, *J. Fluid Mech.* **249**, 135 (1993).
- [8] Y. Liu and R.E. Ecke, *Phys. Rev. Lett.* **79**, 2257 (1997).
- [9] E. King, S. Stellmach, J. Noir, U. Hansen, and J. Aurnou, *Nature* **457**, 301 (2009).
- [10] J.Q. Zhong, R.J.A.M. Stevens, H.J.H. Clercx, , R. Verzicco, D. Lohse, and G. Ahlers, *Phys. Rev. Lett.* **102**, 044502 (2009).
- [11] Y. Liu and R.E. Ecke, *Phys. Rev. E* **80**, 036314 (2009).
- [12] K. Julien, S. Legg, J. McWilliams, and J. Werne, *J. Fluid Mech.* **322**, 243 (1996).
- [13] R.J.A.M. Stevens, J.Q. Zhong, H.J.H. Clercx, G. Ahlers, and D. Lohse, *Phys. Rev. Lett.* **103**, 024503 (2009).
- [14] M. Sprague, K. Julien, E. Knobloch, and J. Werne, *J. Fluid Mech.* **551**, 141 (2006).
- [15] J. M. Pfotenhauer, J. J. Niemela, and R. J. Donnelly, *J. Fluid Mech.* **175**, 85 (1987).
- [16] I. Grooms, K. Julien, J. B. Weiss, and E. Knobloch, *Phys. Rev. Lett.* **104**, 224501 (2010).
- [17] K. Julien, E. Knobloch, A. M. Rubio, and G. M. Vasil, *Phys. Rev. Lett.* **109**, 254503 (2012).
- [18] B. M. Boubnov and G. S. Golitsyn, *J. Fluid Mech.* **219**, 215 (1990).
- [19] E. King, S. Stellmach, and J. Aurnou, *J. Fluid Mech.* **691**, 568 (2012).
- [20] J.-Q. Zhong and G. Ahlers, *J. Fluid Mech.* **665**, 300 (2010).
- [21] J. J. Niemela, S. Babuin, and K. R. Sreenivasan, *J. Fluid Mech.* **649**, 509 (2010).
- [22] J. J. Niemela, L. Skrbek, K. R. Sreenivasan, and R. J. Donnelly, *Nature* **404**, 837 (2000).
- [23] B. M. Boubnov and G. S. Golitsyn, *J. Fluid Mech.* **167**, 503 (1986).
- [24] S. Weiss and G. Ahlers, *J. Fluid Mech.* **684**, 407 (2011).